BIOCHEMISTRY
including biophysical chemistry & molecular biology

Article

pubs.acs.org/biochemistry

Length-Dependent Aggregation of Uninterrupted Polyalanine Peptides

Joseph P. Bernacki and Regina M. Murphy*

Department of Chemical and Biological Engineering, University of Wisconsin, 1415 Engineering Drive, Madison, Wisconsin 53706, United States

ABSTRACT: Polyalanine (polyA) is the third-most prevalent homopeptide repeat in eukaryotes, behind polyglutamine and polyasparagine. Abnormal expansion of the polyA repeat is linked to at least nine human diseases, and the disease mechanism likely involves enhanced length-dependent aggregation. Because of the simplicity of its side chain, polyA has been a favorite target of computational studies, and because of their tendency to fold into α-helix, peptides containing polyA-rich domains have been a popular experimental subject. However, experimental studies on uninterrupted polyA are very limited. We synthesized polyA peptides containing uninterrupted sequences of 7 to 25 alanines (A7 to A25) and characterized their length-dependent conformation and aggregation properties. The peptides were primarily disordered, with a modest component of α-helix that increased with increasing length. From measurements of mean distance spanned by the polyA segment, we concluded that physiological buffers are neutral solvents for shorter polyA peptides and poor solvents for longer peptides. At moderate concentration and near-physiological temperature, polyA assembled into soluble oligomers, with a sharp transition in oligomer physical properties between A19 and A25. With A19, oligomers were large, contained only a small fraction of the total peptide mass, and slowly grew into loose clusters, while A25 rapidly and completely assembled into small stable oligomers of ~7 nm radius. At high temperatures, A19 assembled into fibrils, but A25 precipitated as dense, micrometer-sized particles. A comparison of these results to those obtained with polyglutamine peptides of similar design sheds light on the role of the side chain in regulating conformation and aggregation.

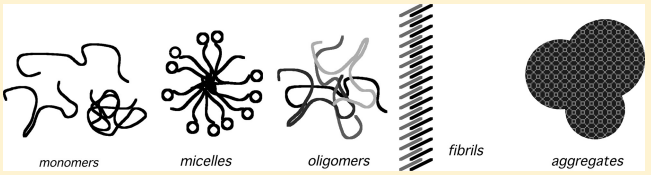

Nearly 500 proteins containing polyalanine (polyA) segments have been identified in humans,[1] making polyA the third-most prevalent homopeptide repeat in eukaryotes, behind polyglutamine (polyQ) and polyasparagine (polyN).[2] Repeats of seven or more alanines are particularly common in transcription factors.[3] Abnormally expanded polyA segments have been linked to nine human diseases, eight of which result in congenital malformations, while the ninth, oculopharyngeal muscular dystrophy (OPMD), is an adult-onset disease.[1,4−6] The disease mechanisms are uncertain, but it is established that expansion of polyalanine tracts can lead to protein misfolding, aberrant protein−protein interactions, cellular mislocalization, and aggregation.[1,5] Several lines of evidence link the aggregation of proteins containing expanded polyA segments to toxicity. PolyA-fusion proteins form toxic aggregates,[7,8] and both aggregation and toxicity can be reduced by overexpression of ubiquitin.[9,10] Treatments that reduced aggregation of the protein implicated in OPMD, polyadenylate binding protein nuclear 1 (PABPN1), also reduced toxicity and morbidity.[11−13] The solubility and toxicity of polyA within the context of a PABN1-like protein are strongly length-dependent, with a sharp transition around 20 alanines.[17] As with other aggregation-related disorders, soluble oligomers are suspected to serve as intermediates in the aggregation process and to be more toxic than mature aggregates.[14,15]

Expanded polyA diseases share some characteristics with the more prevalent expanded polyQ-mediated disorders, but there are distinct differences as well. All known polyQ diseases are late-onset disorders, while symptoms in all but one polyA disease appear at birth. The normal length of the polyA domain tends to be smaller than for polyQ, with a sharper threshold for expansion in the disease phenotype (9−20 residues for polyA with +1-14 expansion, compared to 4-44 with +1-271 expansion for polyQ).[1,4−6,16] Some evidence suggests that expansion of polyA may be more damaging than expansion of polyQ. For example, in a cell model of spinocerebellar ataxia type 7, substitution of polyA for polyQ showed increased toxicity despite similar expression levels and identical repeat length.[18] Interestingly, a polyA-GFP construct in drosophila resulted in toxicity and aggregation at high expression, but low levels of expression triggered a heat shock response that actually protected cells against polyQ-mediated aggregation and toxicity.[19]

Besides their association with expanded-domain disorders, alanine-rich sequences have long attracted interest for fundamental investigations into protein folding, motivating both theoretical and experimental studies of synthetic polyA-containing peptides. PolyA peptides are particularly amenable to molecular dynamics simulations due to the relative simplicity of the alanine side chain.[20,21] The folding properties of polyA-rich peptides, typically containing periodic interrupting residues and/or long helix-promoting flanking residues, have been the

Received: July 26, 2011
Revised: September 20, 2011
Published: September 20, 2011

subject of numerous experimental investigations (e.g., refs 22−26).

In contrast, there are only a few theoretical and experimental studies of peptides with uninterrupted polyA domains or studies that focused on aggregation properties. To simulate aggregation of polyA peptides, Hall and co-workers used simplified descriptors and discontinuous molecular dynamics.[27,28] They observed a complex mixture of species: individual peptides in α-helical or random coil conformation, amorphous aggregates retaining some α-helical structure, individual β-sheets that grow via β-strand addition of individual peptides, and β-rich aggregates formed by the alignment of β-sheets that grow via sheet and strand addition. Other simulations suggest that polyA segments are able to "template" one another into matching conformations.[29,30] Blondelle and co-workers synthesized polyA peptides of varying length (Ac-KYA$_N$K-NH$_2$, with $3 \leq N \leq 25$) and discovered that longer peptides irreversibly formed large, stable, β-sheet rich complexes with fibrillar morphologies;[31−33] conversion of monomeric peptide to aggregates was observed only at high concentrations and temperatures (2−10 mg/mL, 45−65 °C).[34] Giri et al. synthesized a mimic of the N-terminus of PAPBN1, Ac-KMA$_N$GY, and reported that short peptides (N = 7) were α-helical, nontoxic, and nonaggregating, while β-sheet structure and nonfibrillar aggregation were observed for N = 11 and N = 17, but only at high pH.[35,36] Measey et al. observed fibril formation at acidic pH and high concentration (>20 mM) in Ac-A$_4$KAY-NH$_2$.[37] Soluble β-sheet aggregates were observed at pH 2.7 and 5 mg/mL for the alanine-based 16-mer (AAKA)$_4$.[38] In all these studies, aggregates were observed only at highly nonphysiological conditions and/or the polyalanine domain contained non-alanine interrupting residues.

In this work, we synthesized Ac-K$_2$WA$_N$K$_2$-NH$_2$, with N varying from 7 to 25, to study length-dependent conformation and aggregation of peptides with uninterrupted polyalanine domains. Our experiments were conducted at near-physiological pH, temperature, and ionic strength. We endeavored to investigate the early stages of aggregation due to the putative importance of soluble oligomers in the aggregation mechanism and toxicity. Multiscale biophysical techniques were utilized, examining both the conformation of the individual peptides and the characteristics of oligomers and aggregates. Our results provide, for the first time, experimental evidence for soluble oligomer formation in uninterrupted polyA peptides near physiological conditions. We also show that, although there is a smooth increase in helical content and monomer extension with length, there is a sharp transition in aggregate characteristics at $19 < N < 25$. Our data for polyA can be profitably compared to previously published polyQ characterizations[39−41] to examine the role of specific side chains in modulating conformation and aggregation behavior of homopeptide repeats.

MATERIALS AND METHODS

Peptide Synthesis and Purification. All materials were purchased from Fisher Scientific (Pittsburgh, PA), except where indicated. Peptides were synthesized on a NovaPEG Rink amide resin (Novabiochem, Gibbstown, NJ) with a Symphony peptide synthesizer (Protein Technologies, Tucson, AZ). Fmoc-alanine, Fmoc-lysine(boc), and Fmoc-tryptophan(boc) were purchased from Protein Technologies. To avoid problems with on-bead β-sheet folding and aggregation,[42,43] resin sites were partially blocked by manual addition of 1:1 Fmoc-lysine(boc) and boc-lysine(boc). Extended cycles and double couplings were used to improve yields. Peptides were deprotected and cleaved in 95% trifluoroacetic acid (TFA), 2.5% H_2O, and 2.5% ethanedithiol (Sigma-Aldrich, St. Louis, MO) and then precipitated into cold *tert*-butylmethyl ether. Crude peptides were dissolved in a 1:1 mixture of TFA and hexafluoroisopropanol (HFIP). Following evaporation under gentle N_2 flow, the peptide was redissolved in TFA, diluted with H_2O to 10−50% TFA, and then purified by reverse-phase high-performance liquid chromatography (RP-HPLC) on a Vydac C18 column (Grace, Deerfield, IL). Elution with a shallow linear gradient of acetonitrile (ACN) and H_2O was required to resolve impurities. The peak corresponding to the correct molecular weight was collected and lyophilized. Molecular weights of the purified peptides were verified via MALDI-TOF mass spectrometry (1255.9, 1682.2, 2108.0, and 2534.4 for A7, A13, A19, and A25, respectively). For FRET experiments, peptides containing both donor (Trp) and acceptor (dansyl) were synthesized and purified in the same manner, except the C-terminal-most Ala was replaced with dansylated Lys (Anaspec, San Jose, CA).

Sample Preparation. Purified peptides were disaggregated essentially as described elsewhere.[40,44] Lyophilized peptides were dissolved in a 1:1 mixture of TFA and HFIP and incubated for 2 h. The solvent was evaporated under a gentle nitrogen flow, and the peptide was redissolved in H_2O adjusted to pH 3 with TFA to a final peptide concentration of 400−600 μM. This stock solution was aliquoted, snap-frozen, and stored at −80 °C. Prior to each experiment, an aliquot was thawed and centrifuged at 19 500 RCF for 30 min, and the supernatant (top 90%) was immediately diluted into universal buffer (UB). UB contained a total of 0.1 M salt cations (0.05 M each Na^+ and K^+) and 0.1 M buffer anions (0.025 M each citrate, phosphate, tetraborate, and Tris), adjusted to pH 7.0. All buffer stocks were double-filtered at 0.22 μm, and all samples were filtered at 0.45 μm. Peptide concentrations were determined by Trp fluorescence.[40] Briefly, samples were diluted 10-fold into 8 M urea. Tryptophan fluorescence spectra were obtained with a QuantaMaster Series spectrofluorometer from PTI (Birmingham, NJ) with excitation at 295 nm and emission measured from 300 to 580 nm. For concentration determination, emission intensity was compared to a standard curve of pure tryptophan in 8 M urea. To check for changes in the Trp local environment, the derivative of the spectra with respect to wavelength, $dF(\lambda)/d\lambda$, was numerically evaluated to find the wavelength at maximum emission (where $dF(\lambda)/d\lambda = 0$). For dansylated peptides, concentration was checked using dansyl-lysine standards in case of any interference due to FRET.

Circular Dichroism (CD). Each sample (10 μM) was transferred to a 1 mm cell and thermally equilibrated to 25 °C. CD spectra were taken on an Aviv 202SF CD spectrometer from Aviv Biomedical (Lakewood, NJ). Blank solvent spectra were collected and subtracted.

Fluorescence Resonance Energy Transfer (FRET). Tryptophan fluorescence spectra of peptide samples (10 μM) were obtained with excitation at 295 nm and emission from 300 to 580 nm. All spectra was collected at room temperature (22 °C). Mean intensities were determined by integrating the areas under the emission curves from 305 to 410 nm for both peptides with Trp donor only (F_D) and both donor and dansyl acceptor (F_{DA}). Measurements were taken weekly for 6 weeks, but no significant change with time was observed (not shown). Reported data is the average of all measurements. For a fixed

system, the efficiency of the nonradiative energy transfer E from donor to acceptor is a function of the distance R between donor and acceptor:[45]

$$E = 1 - \frac{F_{DA}}{F_D} = \frac{{R_0}^6}{{R_0}^6 + R^6} \quad (1)$$

where R_0 is the Förster radius for a given donor−acceptor pair. We used R_0 = 21 Å for the three smaller peptides based on literature values[46] and R_0 = 23.0 Å for N = 25 from measurement of the spectral overlap integral. For conformationally heterogeneous systems, the measured energy transfer is an average $\langle E \rangle$ over the conformational distribution $P(r)$ and the distance-dependent energy transfer $E(r)$ integrated over the chain length L:

$$\langle E \rangle = \frac{\int_0^L E(r)P(r)\,dr}{\int_0^L P(r)\,dr} \quad (2)$$

Sedimentation Assay. Peptide samples (100 μM) were incubated at room temperature (~22 °C). At regular time intervals, 100 μL aliquots were removed and centrifuged for 30 min at 19 500 RCF. The supernatant was removed, and the concentration was determined in triplicate by fluorescence.

Size-Exclusion Chromatography (SEC). Peptide samples (100 μM) were incubated at room temperature (~22 °C). At regular time intervals, 75 μL aliquots were removed and injected onto a Superdex 75 PC 3.2/30 column (GE HealthCare Life Sciences, Piscataway, NJ) using a 50 μL sample loop and UB as the mobile phase. Peaks were detected by absorbance at 280 nm, and peak area was obtained by integration, with baseline correction. Fractional recovery was calculated by dividing the area of the monomer peak by the peak area of a sample injected without the column in place.

Light Scattering. Peptide samples (100 μM) were filtered into a scrupulously cleaned light-scattering cuvette and then placed into a 25 °C bath of the index-matching solvent decahydronaphthalene. Light scattering data were collected using a Brookhaven BI-200SM research goniometer and laser light scattering system (Brookhaven Instruments Corp., Holtsville, NY) and an Innova 90C-5 argon laser (Coherent, Santa Clara, CA) operating at 488 nm wavelength and 150 mW output. The aperture to the photomultiplier was set to 200 μm for the DLS experiments and 400 μm for SLS experiments. Background and reference scattering data were collected from analogously prepared buffer and toluene samples.

For dynamic light scattering (DLS), the autocorrelation function at 90° scattering angle was collected, using 101 channels and a geometric series of delay times. The z-averaged hydrodynamic radius $\langle R_H \rangle$ was determined from the autocorrelation function by the method of cumulants.

For static light scattering (SLS), total scattering intensity at 23 angles (20°−110°) was measured. Three repeats of 1 s duration were collected at each angle, and the data collection was repeated four times, using a freshly prepared sample for each run. A dust rejection algorithm was used to eliminate spurious measurements, and the Rayleigh ratio $R_s(q)$ was calculated at each scattering vector q as described.[47] $R_s(q)$ is related to the weight-averaged molecular weight $\langle M \rangle_w$ and the light-scattering-averaged particle shape factor $P_z(q)$:

$$\frac{R_s(q)}{Kc} = \langle M \rangle_w P_z(q) \quad (3)$$

where c is the mass concentration of the solutes (g/mL) and K is an instrument constant. Equation 3 is true in the limit of low B_2c, where B_2 is the second virial coefficient. Functional equations for $P_z(q)$ for a number of common shapes are known.[48−50] $\langle M \rangle_w$ and $P_z(q)$ were determined as follows. First, estimates of $\langle M \rangle_w$ and the z-averaged radius of gyration $\langle {R_g}^2 \rangle_z^{1/2}$ were obtained by Zimm analysis. These estimates were used as initial guesses in regression of eq 3 to the data, using particle shape factors for nine different shapes (solid sphere, hollow sphere, thin disk, rigid rod, circular cylinder, Gaussian coil, wormlike chain, Gaussian star, and wormlike star). Best-fit parameter estimates for each particle shape were obtained using the software package Athena Visual Studio 14.2 (Athena Visual Software, Naperville, IL), and the best particle shape was chosen using the posterior probability share method.[51] $\langle {R_g}^2 \rangle_z$ was then calculated from the fitted $P_z(q)$ as

$$\langle {R_g}^2 \rangle_z = \lim_{q \to 0} \left(\frac{3q}{2} \frac{\partial}{\partial q} {P_z}^{-1}(q) \right) \quad (4)$$

Transmission Electron Microscopy (TEM). Peptide samples (100 μM) were incubated for ~2 weeks at room temperature (~22 °C). A drop of each sample was applied to a Pioloform-coated grid and stained with methylamine tungstate stain. The sample was then imaged with a Philips CM120 scanning transmission electron microscope from FEI (Hillsboro, OR).

RESULTS

Synthesis of PolyA Peptides. PolyA peptides of the form Ac-$K_2WA_NK_2$-NH_2 were synthesized, where N = 7, 13, 19, or 25. Peptides will be referred to as A7, A13, A19, and A25, respectively. Two flanking lysines were added to the alanine core to increase solubility. Tryptophan was used as a FRET donor and to determine concentration. For FRET experiments, the C-terminal alanine was replaced with the acceptor dansyl. PolyA-rich peptides are prone to formation of interpeptide β-sheet structures during on-bead synthesis.[42,43,52] Previous researchers, in synthesizing similar long uninterrupted polyA peptides, reported that less than 10% of the crude peptide was monomeric and that much was trapped in β-sheet oligomers that eluted as broad peaks.[32,33] We developed our synthesis and purification protocol to avoid these problems. RP-HPLC chromatograms yielded sharp peaks, with the main peak corresponding to the correct sequence as verified by mass spectrometry (data not shown). Minor peaks were typically due to alanine deletions but occasionally to lysine deletions or alanine additions. The major peak was isolated, and the purified peptide was used for all subsequent experiments. We developed a rigorous disaggregation method to ensure that all starting materials were monomeric. No loss of material was ever detected during centrifugation of the disaggregated peptide stock, and the peptide stocks (at pH 3) scattered no light above background as measured by laser light scattering (data not shown). This was interpreted as evidence for successful disaggregation of the stock solutions. There was no loss of material upon filtration after the peptide stocks were diluted into buffer (data not shown).

Effect of PolyA Length on Secondary Structure. CD spectra for freshly prepared solutions of A7, A13, A19, and A25

(10 μM peptide, pH 7, 0.1 M salts) were collected (Figure 1). The fraction of residues in α-helical conformation f_α was

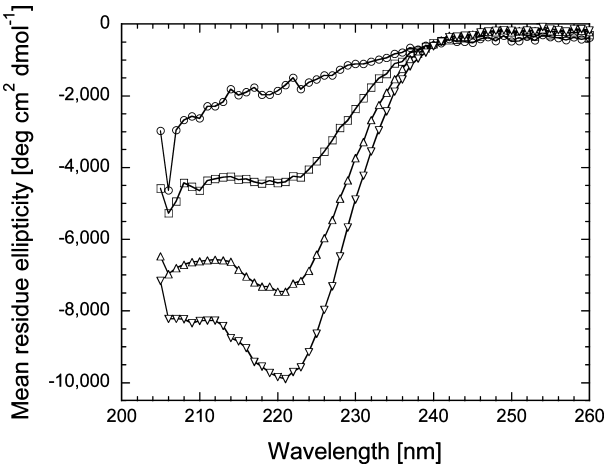

Figure 1. CD spectra for 10 μM polyA in UB: A7 (○), A13 (□), A19 (△), and A25 (▽).

calculated from

$$f_\alpha = \frac{[\theta]_{222} - [\theta]_{222,RC}}{[\theta]_{222,\alpha} - [\theta]_{222,RC}} \quad (5)$$

We set the convergent core ellipticity $[\theta]_{222,\alpha}$ for the fully α-helical core to −54 520 deg cm^2 dmol^{-1} [53,54] and used the A7 ellipticity for $[\theta]_{222,RC}$ (thus assuming that A7 is fully disordered). Using this approach, we calculated α-helicities of 5%, 11%, and 15% for A13, A19, and A25, respectively. The value of f_α depends significantly on the assumed convergent core ellipticities. Using values of −26 000 and −3500 deg cm^2 dmol^{-1} for $[\theta]_{222,\alpha}$ and $[\theta]_{222,RC}$, respectively, as suggested by another group,[55] we obtained values of f_α = −9%, 3%, 17%, and 28% for A7, A13, A19, and A25. The negative value for f_α of A7 might indicate that this peptide samples polyProII (P_{II})-like conformations. Using these calculated values as a range, we conclude that there is no α-helical character to A7, ∼1 residue in α-helical conformation in A13 (averaged over the entire population), 3−4 α-helical residues in A19, and 5−8 in A25.

All samples were incubated at room temperature for 14 days. CD spectra taken after aging were not significantly different (data not shown). To check for concentration-dependent changes in secondary structure, A25 was prepared at 100 μM and then diluted to 10 μM; CD spectra were collected immediately after dilution and were the same as the freshly prepared sample at 10 μM (data not shown).

Our data are generally consistent with other literature reports, although we observed moderately less α-helix, possibly due to the flanking lysines.[56] For example, we analyzed published CD spectra and calculated, using eq 5, that Ac-KMA_7GY and Ac-$KYA_{13}KNH_2$ were 5% and 20% α-helical, respectively.[32,35,57] Two other uninterrupted polyA peptides, containing 12 or 13 alanine residues, were reported to contain 22−25% α-helix.[56,58] In another study, no α-helicity was observed in an A_7 peptide, although residues may sample P_{II}-like conformations.[59,60] A_4 and A_5 were predicted to contain about 75% P_{II} character in one simulation,[61] while another investigator predicted that a length-dependent crossover to α-helix occurs at A_7.[62] Other simulations have yielded estimates of roughly 10% helical content for A_8 and A_{10} and about 25% for A_{14} and A_{15}.[63,64]

PolyA Chain Dimensions. We used FRET to find the average distance between donor and acceptor placed on the termini of the polyA core, reasoning that this distance will describe whether polyA is relatively well- or poorly solvated in aqueous buffer. $\langle R \rangle$ was calculated using FRET data and eq 1; results are shown in Figure 2. All polyA peptide monomers are

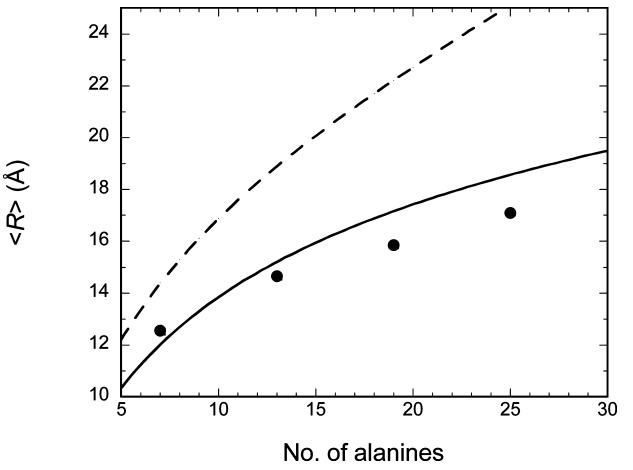

Figure 2. FRET analysis of peptide conformation. Data were obtained for 10 μM polyA in UB. Error Experimental $\langle R \rangle$ values (●) are compared to expected values for a freely jointed chain at the theta condition χ = 0.5 (solid line) and a chain with excluded volume (χ = 0, dashed line). Error bars for experimental values are smaller than the symbol size.

relatively compact rather than extended. For example, for A7, $\langle R \rangle$ = 12.6 Å, compared to a calculated value of 23.8 Å for a peptide of equivalent length in a fully extended β-strand. The increase in $\langle R \rangle$ with polyA length is very small, with $\langle R \rangle \propto N^{0.24}$. This scaling is less than one expects for spheres, indicating that the peptides become more compact as N increases.

To further interpret these data, we calculated the anticipated $\langle R \rangle$ using eqs 1 and 2 and assuming that polyA adopts the conformational distribution

$$P(r) = 4\pi r^2 \exp\left(- \frac{3r^2}{2nl_b^2} - \frac{n^2 v_c}{2r^3}(1 - 2\chi) \right) \quad (6)$$

where l_b is the length of one residue (3.8 Å), n the number of residues, v_c the excluded volume ($\sim l_b^3$), and χ the Flory−Huggins parameter.[65,66] χ was set equal to 0 or to 0.5; the former corresponds to the freely jointed chain with excluded volume while the latter corresponds to the theta condition where excluded volume effects that expand the chain are exactly counteracted by unfavorable solvent−solute interactions that collapse the chain. χ > 0.5 indicates a poor solvent. (Equation 6 is rigorously accurate only for long chains, and so our analysis should be considered only semiquantitative.) A comparison of experimental with calculated $\langle R \rangle$reveals that A7 falls between the two calculated curves, whereas A13, A19, and A25 are both below the theta condition curve (Figure 2). Thus, if we interpret these data in terms of an effective χ, we conclude that χ < 0.5 for A7, and χ becomes increasingly greater than 0.5 for A13, A19, and A25.

dx.doi.org/10.1021/bi201155g | Biochemistry 2011, 50, 9200−9211

The wormlike chain model has been used to describe unfolded polypeptides as well as flexible linkers within multidomain folded proteins.[67,68] As another point of comparison, FRET data were used to estimate an effective persistence length l_p, a measure of the stiffness of the chain. For polyA peptides, l_p varied smoothly from 3.5 Å for A7 to 2.2 Å for A25. This compares to estimates of $l_p \sim 3$ Å for loops in folded protein and for an amphipathic peptide.[68,69] For unfolded proteins and polypeptides, measured persistence lengths typically range from 4 to 9 Å.[40,70,71] We conclude that polyA monomers are compact compared to "average" unfolded proteins, with a segment density closer to folded proteins.

We are aware of only one other study of polyA extension under physiological conditions: FRET measurements of A_5 yielded an effective $\langle R \rangle = 11$ Å,[61] very much in line with our measurement of $\langle R \rangle = 12.6$ Å for A7. Tzul et al. reported that polyA domains in denatured proteins behave as random coils with excluded volume, as measured by kinetics of loop formation.[72] Zhou and co-workers predicted that R_g is 11.5–12 Å for A_{15} from simulations,[73] corresponding to $l_p \sim 7$ Å. This comparison indicates that the solvent properties used in that simulation are not reflective of typical aqueous buffers.

PolyA Aggregate Size and Morphology. Stock solutions (pH 3, no salt) of polyA peptides were first rigorously disaggregated to ensure that starting material was fully monomeric. Then, stocks were diluted into buffer (pH 7.0, 0.1 M salts) to a final peptide concentration of 100 μM and incubated at room temperature (~22 °C) for 6 weeks. None of the samples became turbid, and none were positive for thioflavin-T, a dye commonly used to detect amyloid fibrils. Within experimental error, all of the peptide remained in the supernatant after centrifugation (data not shown).

Both freshly prepared and aged peptide samples were analyzed by SEC. Elution chromatograms for freshly prepared samples are displayed in Figure 3. A7, A13, and A19 all eluted as well-behaved monomers, as indicated by single Gaussian peaks with elution time varying in the order of decreasing molar mass. There was little loss of material (90–95% recovery in monomer peak), with no change over 35 days (not shown). In contrast, A25 eluted with a broad and asymmetric peak and a delayed elution volume. This effect is most likely due to hydrophobic interactions between A25 and the SEC column.[74]

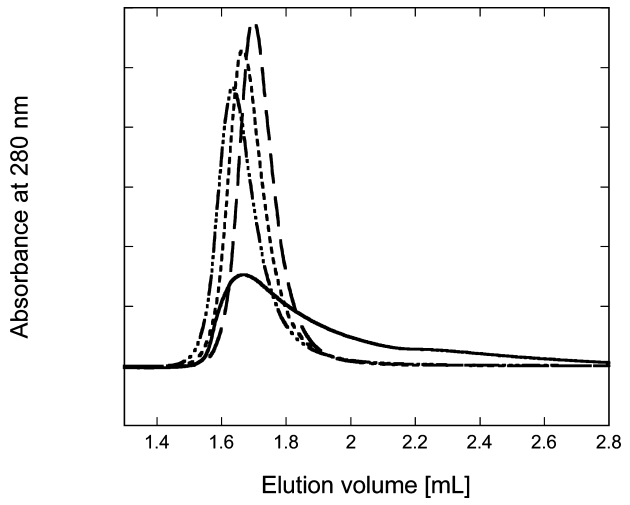

Figure 3. SEC analysis of polyA peptides. Samples were prepared at 100 μM in UB. Chromatograms obtained from freshly prepared samples. Peak detection was by absorbance at 280 nm. The nominal molecular weight range of the column is 3000–70 000, and the included volume is 2.4 mL. A7 (dashed line), A13 (dotted line), A19 (dash-dotted line), and A25 (solid line).

Further evidence of a distinct difference between A25 and shorter peptides was obtained with Trp fluorescence studies. Aged samples (100 μM) were diluted 10-fold into 8 M urea, and their Trp fluorescence emission was measured. With A25, the Trp spectra was blue-shifted significantly ($\lambda_{max} = 345$ nm for A25 versus 351 for others), indicating burial in a hydrophobic environment. There was no blue shift for any of the four peptides if freshly prepared or kept at low concentrations, implying that this is an aggregation-driven phenomenon. Together with the SEC results, these data indicate a sharp length-dependent transition in properties of polyA between $N = 19$ and 25.

We next analyzed polyA solutions by light scattering. In stock solutions (pH 3, no salt), none of the samples scattered light above background. Upon dilution into buffer (100 μM peptide, pH 7.0, 0.1 M salts), scattering above background was detected, indicating the presence of soluble aggregates in all samples. Given the SEC analysis, the fraction of peptide in A7, A13, or A19 incorporated into the soluble aggregates is very low. Detection by SEC of a small fraction of aggregates is particularly problematic if the aggregates are a broad distribution of sizes and/or if the aggregates tend to adsorb to the column. The inability to detect these aggregates by SEC can be attributed to the much greater sensitivity of light scattering to aggregates.

Scattering intensity, which in general increases with increasing number and size of aggregates, increased in the order A13 < A7 < A19 < A25 (Table 1). We collected dynamic light scattering data at 90° scattering angle and analyzed autocorrelation functions using cumulants analysis to determine a mean hydrodynamic radius $\langle R_H \rangle$. Results are summarized in Table 1. Curiously, the largest size particles were obtained with the intermediate polyA lengths (A13 and A19), whereas the smallest particles by far were observed with A25. In all cases, distributions were very broad, as deduced by CONTIN analysis (not shown), indicating the aggregate population is polydisperse. To further analyze the size of soluble aggregates, we collected multiangle scattering data for A7, A19, and A25 (data quality for A13 was poor due to weak scattering and will not be discussed). Data were fitted to eq 3, and the "best" fit particle shape and size parameters were determined (Table 1).

To examine whether there was a change in aggregate size with time, we collected DLS data over several hours (Figure 4). A7 aggregates grew slightly over a few hours and then stabilized, from $\langle R_H \rangle \sim 60$ nm initially to a steady state value of ~85 nm. With A25, $\langle R_H \rangle$ remained steady at 6.5–7 nm. In sharp contrast, the increase in $\langle R_H \rangle$ for both A13 and A19 was significant; the rate of increase was remarkably similar and did not slow much even after several hours.

Electron microscope images of the peptide samples taken after 2 weeks aging at 22 °C are shown in Figure 5. Morphological characteristics varied significantly as a function of polyA length. A7 contained sparse, small, roughly spherical aggregates (15–50 nm), which occasionally associated into long flexible chains with a "pearl necklace" appearance (Figure 5a). Slightly larger spherical aggregates were observed in A13 and A19, but these tended to associate into larger, loose, globular clusters (Figure 5b,c). Clusters were much more

Table 1. Light Scattering Analysis of PolyA Peptide Aggregation[a]

no. of alanines N	$I_{norm}(90°)$[b]	$\langle R_H \rangle$[d] (nm)	$\langle M \rangle_w$ (kDa)	best-fit shape	$\langle R_g^2 \rangle_z^{1/2}$[c] (nm)
7	61	54	520 ± 20	rod/coil	55
13	52	115	ND[e]	ND	ND
19	160	143	2500 ± 150	coil	184
25	212	7	500 ± 20	ND[e]	ND

[a]Data taken within 5 min or less of dilution into buffer (pH 7.0, 0.1 M salts, 100 μM peptide). [b]Scattering intensity at 90° angle, normalized to mass concentration. Units are 1000 counts/s per mg/mL. [c]$\langle R_g^2 \rangle_z^{1/2}$ is calculated from eq 4 for the best-fit particle shape. [d]$\langle R_H \rangle$ is the inverse-z-averaged hydrodynamic radius from cumulants analysis of autocorrelation data. CONTIN analysis of the same data yielded nominally larger mean radii. [e]Not determined. For A13, scattering was too weak to obtain reliable angle-dependent data. For A25, particle shape could not be discriminated because of small particle size.

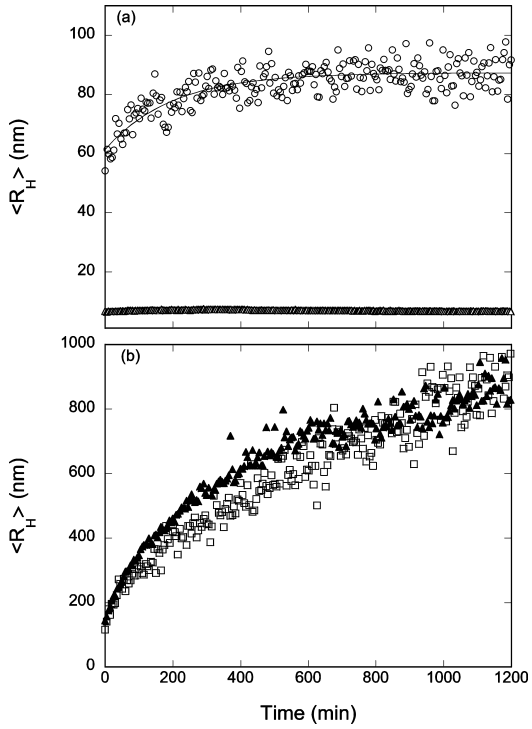

Figure 4. Kinetics of aggregation. Samples were prepared at 100 μM in UB, and apparent hydrodynamic radius $\langle R_H \rangle$ was measured over time using dynamic light scattering with cumulants analysis. (a) A7 (○) and A25 (△). (b) A13 (□) and A19 (▲). Data are representative of 3−4 repeats.

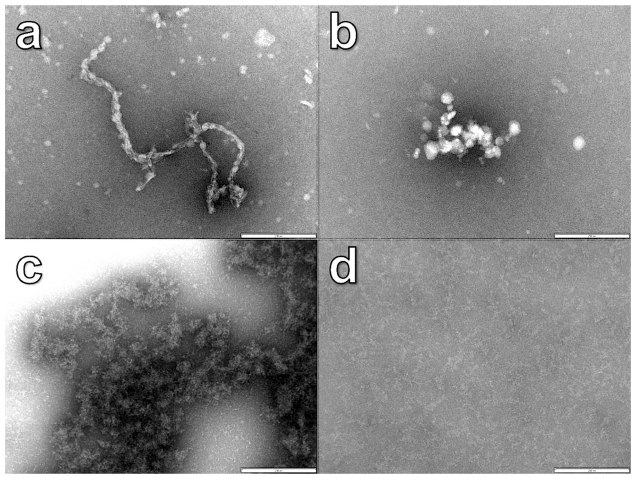

Figure 5. Transmission electron microscope images of polyA peptide aggregates at 25 °C. Samples were prepared at 100 μM peptide in UB and incubated at 25 °C for ~2 weeks prior to imaging. All images are representative of a large number of images from multiple samples. Scale bar: 200 nm. (a) A7, (b) A13, (c) A19, and (d) A25.

numerous in A19 compared to A13. In sharp contrast, no aggregates were observed in the A25 samples. Rather, the sample appeared as a mottled film when dried on the grid (Figure 5d).

From the combined SEC, fluorescence, light scattering, and EM data, a picture emerges of the properties of polyA aggregates as a function of length. The data for A25 aggregates may be the most straightforward to interpret. If we assume that all A25 is incorporated into spherical aggregates of $\langle M \rangle_w = 5.2 \times 10^5$ Da (Table 1), we can estimate the hydrated volume $\langle V_H \rangle$ from

$$\langle V_H \rangle = \frac{4\pi}{3}\langle R_H \rangle^3 = \frac{\langle M \rangle_w}{N_A}(V_p + \delta V_w) \quad (7)$$

where N_A is Avogadro's number, V_p and V_w are partial specific volumes of peptide and water, respectively, and δ is the grams bound water/gram peptide. V_p and δ are calculated from the amino acid composition[75,76] and equal 0.756 cm^3/g and 0.43 g/g, respectively, for A25. This yields an estimate of $\langle V_H \rangle \sim 1030$ nm^3, or $\langle R_H \rangle \sim 6.3$ nm, very close to the hydrodynamic radius measured by dynamic light scattering (Table 1). Thus, we interpret these data to indicate that A25 readily assemblies into stable, compact oligomers with densities approaching that of folded proteins. This interpretation is consistent with the lack of monomer peak on SEC and with the shift in Trp environment upon aggregation.

Aggregates of A7, A13, and A19 clearly differ from A25. $\langle M \rangle_w$ for A7 and A25 are virtually identical, but $\langle R_H \rangle$ is 8-fold larger for A7. Similarly, $\langle M \rangle_w$ for A19 is 5-fold greater than for A25, but $\langle R_H \rangle$ is more than 20-fold larger. Furthermore, A7, A13, and A19 elute largely as monomers on SEC, whereas the A25 elution profiles are distorted. These data can be understood if we take into account two considerations. First, $\langle M \rangle_w$ is the weight-averaged molecular weight for all particles in solution while $\langle R_H \rangle$ is weighted toward larger particles. If we assume that the particles in solution are a mix of monomer and aggregate, then

$$\langle M \rangle_w = \sum w_i M_i \cong w_m M_m + w_{agg} M_{agg} \quad (8a)$$

where w_i and M_i are the weight fraction and molecular weight, respectively, of species i, and subscripts m and agg indicate

dx.doi.org/10.1021/bi201155g | Biochemistry 2011, 50, 9200−9211

monomer and aggregate, respectively. If we further assume that $M_{agg} \gg M_m$, then

$$\langle M \rangle_w \cong w_{agg} M_{agg} \quad (8b)$$

We do not have a direct measure of w_{agg} but conclude from SEC that most (at least 90−95%) of A7, A13, and A19 remain monomeric. Thus, M_{agg} for A7, A13, and A19 is at least 10−20-fold larger than $\langle M \rangle_w$ and would therefore be expected to have a larger hydrodynamic radius. Second, "looser", extended, or more hydrated aggregates occupy a much larger hydrodynamic volume per mass than compact aggregates. From particle shape analysis of SLS data, we conclude that for A7 and A19 aggregates are not compact solid spheres but are more expanded. This is confirmed by examining TEM images, where large, loose clusters of aggregates were observed. In agreement, the increase in $\langle R_H \rangle$ over time for A13 and A19 (Figure 4) is consistent with a continuing association of smaller aggregates into clusters.

Effect of Temperature and Salt. We incubated A19 and A25 at 60 °C. Both solutions became turbid within a day or less: A19 formed a cloudy suspension whereas A25 precipitated. After 5 days, the samples were examined by EM. Surprisingly, A19 formed fibrillar aggregates, several micrometers long, some with an apparent twist (Figure 6a). These fibrillar aggregates are strikingly similar in appearance to polyQ aggregates at room temperature.[40] On the other hand, A25 formed very large (∼5 μm), dense, and more-or-less spherical agglomerates (Figure 6b). We also tested the effect of salt concentration by doubling the tetraborate concentration (from 0.025 to 0.05 M). Monomer conformation, as measured by FRET and CD, was not affected (data not shown). By DLS and EM, we observed no change in A19 aggregation kinetics or morphology (not shown). In contrast, A25 was remarkably affected by this small change in salt: after a short delay the peptide aggregated quickly and precipitated into larger (∼5 μm) agglomerates, similar in appearance to those generated at high temperature. These data highlight again another striking difference in aggregation behavior below and above $N = 20$.

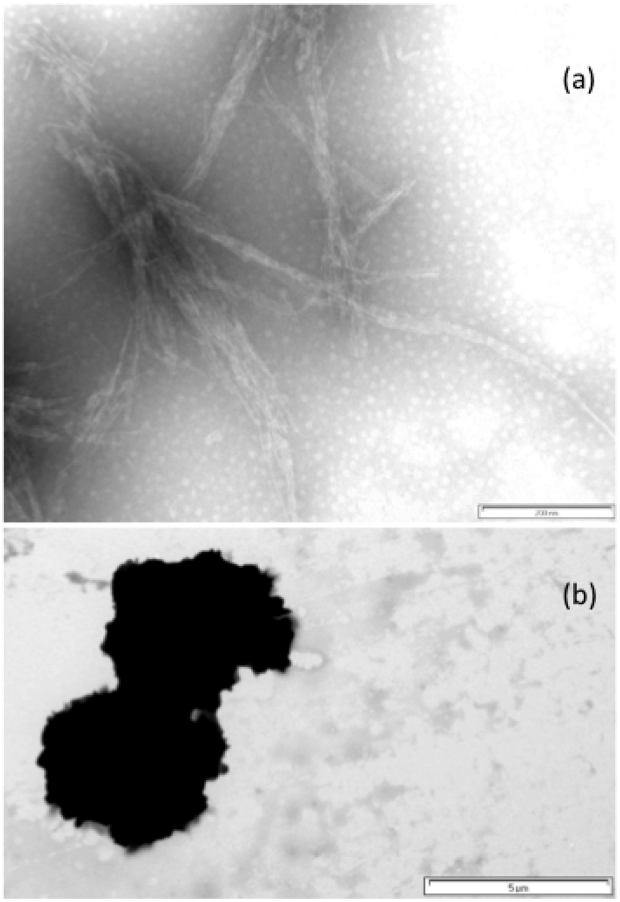

Figure 6. Transmission electron microscope images of polyA peptide aggregates at 60 °C. Samples were prepared at 100 μM peptide in UB and incubated at 60 °C for ∼2 weeks prior to imaging. All images are representative of a large number of images from multiple samples. (a) A19. Scale bar: 200 nm. (b) A25. Scale bar: 5000 nm.

DISCUSSION

We report the systematic study of length-dependent changes in conformation and aggregation of peptides containing uninterrupted polyalanine. There is a paucity of experimental data describing properties of such peptides, despite their connection to human diseases involving abnormally expanded polyA domains. Blondelle and co-workers[31−34] observed conversion of partially helical polyA monomers to soluble β-sheet-rich oligomers, but only at high concentration (∼500−1000 μM or greater) and high temperature (55−65 °C). Conversion was length-dependent; no aggregates were observed with short ($N < 8$) peptides, while long ($N > 15$) peptides were completely aggregated. Other groups observed fibril formation with polyA-containing peptides ($N = 11$ and 17), but only at high pH,[35,36] or at acidic pH and high concentration.[37] Our results are the first, to our knowledge, to demonstrate the presence of soluble aggregates for uninterrupted polyA peptides at near-physiological temperature and pH, which we believe we were able to detect by using sensitive DLS and SLS techniques.

PolyA Secondary Structure and Conformation. Uversky et al.[77] proposed a simple relationship for predicting whether a polypeptide sequence would fall into the intrinsically disordered or natively folded regime, with low hydrophobicity and high net charge favoring intrinsic disorder. Extrapolating this relationship to our peptides, we find that A7 is borderline, whereas A13, A19, and A25 are in the native regime. Counterbalancing the drive for folding is the relatively short lengths of our peptides as well as their low complexity. Ensembles of conformations rather than unique folds arise from low-complexity sequences because there are many energetically equivalent conformations in homorepeats.[78]

Results we obtained from CD and FRET experiments can be profitably examined within this framework. We observed a nearly linear increase in α-helical content, from 0 to about 5−8 residues, as polyA segment length was increased from 7 to 25. Still, even A25 was mostly (∼75%) disordered. In aqueous solution, polyA peptides, especially the longer ones, behaved as compact globules rather than extended coils. The observation that polyA peptides are collapsed is not surprising, as water is a poor solvent even for more hydrophilic homorepeats such as polyglycine.[78] Our analysis of the FRET data suggests that solvent−solute interactions became increasingly unfavorable with increasing alanine length, with estimates of effective $\chi < 0.5$ for A7 and $\chi > 0.5$ for A13, A19, and A25. This worsening of solvent quality with length can be attributed to both increasing mean hydrophobicity and decreasing mean charge. This analysis suggests that the equation developed by Uversky defines a border between good and poor solvents. Polyalanine

peptides such as A25 for which water is a poor solvent fall into the "native" regime;[77] they attain densities approaching natively folded proteins but their low complexity precludes attainment of a single uniquely defined secondary structure. As polyA length increases, excluded volume becomes less significant, which yields a change in globule shape from ellipsoidal to nearly spherical.[79] Tran et al.[78] considered the behavior of polyglycine in terms of the "blob" model and estimated that a "blob" is equivalent to 2−3 residues. Given this estimate, A7 is about 2 "blobs", too small to collapse into a sphere and more like a "sausage". On the other hand, A25 is about 10 "blobs" and thus should be sufficiently long to fully collapse.[78]

Aggregation of Polyalanine. Although the properties of polyA monomers changed only gradually with length (Figures 1 and 2), there was a sharp length-dependent transition in aggregation, as demonstrated by the combined SEC, DLS, SLS, and EM results. Briefly, for N = 7, 13, or 19, a small fraction of peptide rapidly associates into roughly spherical oligomers upon dilution into physiological buffer (room temperature, 100 μM peptide). For A7, a few of these oligomers further coalesce into long, ropelike aggregates ~1 μm in total contour length. For A13 and A19, these oligomers associate together slowly into large, loose clusters. By both EM and LS, aggregates were more numerous in A19 than in A13.

Aggregates of A25 differed fundamentally from those of the three shorter peptides. They were much smaller ($\langle R_H \rangle \sim 7$ nm), and the size remained stable over time. No discrete aggregates were observed by EM (Figure 5d), consistent with the small $\langle R_H \rangle$ because aggregates with features of this size would be difficult to observe on standard TEM. Unlike A7, A13, and A19, no monomer peak was isolated by SEC for A25; the broad and distorted elution profile along with the Trp fluorescence shift indicates a qualitatively different assembly process. Close agreement between $\langle R_H \rangle$ calculated from $\langle M \rangle_w$ and $\langle R_H \rangle$ measured by DLS suggest that virtually all A25 associates into compact oligomers, with densities approaching proteins, yet with only a small content of regular secondary structure.

Natively unfolded polypeptides have greater plasticity than folded proteins, which could be advantageous for permitting interactions with multiple target proteins.[77,80] This promiscuity of interaction includes the possibility for self-interaction. Our data show that a small fraction of A7, A13, and A19 weakly self-associates into large, hydrated, and heterogeneous oligomers that can undergo further agglomeration into larger clusters. The extent of self-association, and the morphology of the clusters, may depend on the balance between hydrophobic interactions and electrostatic repulsion as well as the shape of the underlying monomeric globule. One can envision for example how the A7 "sausage" might align into a "rope". In contrast, we hypothesize that A25, due to its more "native" behavior, is able to self-assemble into small stable oligomers in a process that may be more akin to the attainment of quaternary structure in multimeric proteins.

Interestingly, at high temperatures, A19 associated into fibrillar rather than amorphous aggregates. Within the nonpolar interior of an aggregate, alanines may "dissolve" each other and become extended rather than collapsed. Blanch et al.[81] reported that heating of an alanine-rich peptide caused a conversion from helix to the more extended and flexible P_{II} conformation, which he linked to amyloid prefibrillar intermediate. Thus, high temperatures may allow "melting", rearrangement, and extension of the polyA domain within the aggregate, leading to the more ordered fibrillar aggregates that we observed with A19. Strikingly, though, A25 did not convert to fibrils at high temperature but rather coagulated into very large, dense particles. One possibility is that A25 is too "folded" to rearrange into fibrils: A25 oligomers constitute a suspension of colloidal particles with hydrophobic surfaces that, when placed in an environment that strengthens hydrophobic interactions (high T or salt), simply flocculate.[82]

Comparison to Simulations. In simulations of polyA aggregation, Nguyen and Hall observed rapid coalescence of monomers into amorphous oligomers that contained some α-helix.[27] Small oligomeric β-sheets eventually emerged from these amorphous aggregates; these β-sheets then grew into fibrils by both elongation through β-strand addition and lateral β-sheet addition.[27,28] Fibril formation was favored in the simulations at high concentration and moderately high temperature. Nguyen and Hall noted that increasing the value of a key adjustable parameter, the relative ratio of hydrophobic strength to hydrogen bonding, traps the aggregates in an amorphous rather than fibrillar aggregate state.[27] Our data suggest that polyA peptides containing between 7 and 25 alanines are indeed trapped as amorphous, nonfibrillar oligomers at room temperature. At high temperature, A19 associated into fibrillar rather than amorphous aggregates, in qualitative agreement with the Nguyen and Hall simulations. Blondelle and colleagues likewise found that high temperature was required to force fibril formation and growth.[34]

Dill and co-workers[83] have recently proposed a simple description of the equilibrium between monomers, oligomers (in which the monomer chains are clustered via hydrophobic collapse but are disordered), and fibrils:

$$c_t = c_m + pc_{oligo} + qc_{fibril} = c_m + pc_m{}^p \exp(\chi pN) + \gamma^{bl} \sum qc_m{}^q g^{qN} \quad (9)$$

where c_m is the monomer concentration at equilibrium, p is the number of monomers in the oligomer, q is the number of monomers in fibril bundle, γ is related to the energy associated with initiating zipping at the edge of the β-sandwich, b is the number of β-sandwiches in the fibril, l is the length of β-strand in fibril, and g is the dimensionless equilibrium constant for propagation of the β -strand within the fibril.

We used eq 9 to compare this model to our data. The total concentration c_t is calculated by dividing the peptide concentration (in M) by the molarity of water. We assumed that only alanines were involved in oligomer formation, so N = 7, 13, 19, or 25. The number of chains in each oligomer is not known; we somewhat arbitrarily chose p = 10. At room temperature, no fibrillar aggregates were observed, so the third term on the right-hand side was set equal to zero. Using these values, we calculated from eq 9 that, at 10 μM, there are essentially no oligomers present for any peptides, whereas at 100 μM, there are virtually no oligomers for A7, A13, or A19, but about 65% accumulation of peptide into oligomers for A25. Though the results from these calculations depend strongly on the assumed value of p, this simple model captures the sharp length-dependent transition observed experimentally.

Can this model explain why A19 forms fibrils at high temperatures but A25 does not? Necessary conditions for fibril formation are $g > 1$ and $\chi < \ln g$.[83] If g is not much greater than 1 (say, g = 1.7), then a modest increase in χ with increasing N (say, from 0.5 to 0.55 as N increases from 19 to 25) would

mean a switch from fibrils to oligomers. Similarly, the switch from oligomers to fibrils for A19 with increasing temperature could arise from a small increase in g (or a decrease in χ) with temperature. Recent theoretical studies describe the diversity of morphologies possible in aggregates of peptides containing polyA domains.[84] Such theoretical investigations might prove fruitful in explaining the underlying physical processes behind our observations and more empirical models such as that embodied in eq 9.

Comparison of PolyA to PolyQ. We previously completed similar studies with polyQ peptides of similar design and length.[40,41] A comparison of the two may shed light on the specific role of the side chain chemistry in directing conformation and aggregation. Glutamine's amide side chain is generally considered hydrophilic and is capable of participating in hydrogen bonds as both a donor and acceptor. Our polyQ peptides lie well within the predicted "intrinsic disorder" regime.[77] From CD spectra, polyQ peptides lacked regular secondary structure (other than some P_{II}) across the entire length span; there was no evidence for α-helix formation, unlike polyA. FRET analysis yielded the result that polyQ is more extended in aqueous buffers than polyA, with $l_p \sim 6$ Å (although decreasing with increasing Q length) compared to 2−3 Å for polyA. Like polyA, polyQ rapidly formed large soluble aggregates immediately upon dilution into physiological buffers, but only for $N \geq 16$.[40] Unlike polyA, sedimentable aggregates formed with polyQ ($N \geq 16$) after a short lag time and eventually a large fraction of the material sedimented. By EM, polyQ aggregates were clearly fibrillar in morphology, and mature aggregates appeared as organized bundles of laterally aligned fibrils,[40] while polyA aggregates were clearly nonfibrillar and amorphous (Figure 5).

We previously proposed that polyQ peptide aggregation proceeds via association into soluble oligomers, followed by structural rearrangement within the oligomer to an ordered aggregate with β-sheet hydrogen-bonding patterns and fibrillar morphologies.[40] Conversion from the disordered oligomer to ordered fibril is presumed to be driven by additional hydrogen bonding and ordered hydrophobic interactions, but hindered by loss of conformational entropy and disordered hydrophobic interactions. Important differences in the alanine and glutamine side chains lead to differences in the relative contributions of these interactions. We can compare Q24 (which forms fibrils[40]) to A25. Q24 lacks regular secondary structure, whereas A25 has partial α-helical content. Thus, in forming β-sheet fibrils, Q24 would gain stabilizing backbone−backbone hydrogen bonds while A25 would see little net enthalpy change because α-helix hydrogen bonds would need to be broken to gain β-sheet. (This would be less of a factor for A19 because the monomer contains less α-helix.) Unlike polyQ, polyA would gain no enthalpic benefit from side chain-side chain hydrogen bonds by forming ordered aggregates but would still suffer the entropic penalties associated with decreased conformational freedom. Additionally, alignment of the long glutamine side chains in β-sheets would improve steric packing and allow greater regular contact between the $-CH_2-CH_2-$ moieties on glutamine side chains and thus enhanced hydrophobic interactions, whereas any increased favorable hydrophobic interactions or improved steric packing with the small $-CH_3$ of alanine via backbone alignment is likely to be minor. In the context of eq 9, this line of reasoning would support a higher g for polyQ than for polyA and, from previously published FRET data, a lower χ. Thus, one expects fibrils are strongly favored over soluble oligomers for polyQ at equilibrium.

Effect of Flanking Lysines. Lysines flanking the polyA domain were necessary to overcome synthesis issues and to facilitate initial solubilization. However, the added charge from these flanking residues likely influences conformation and aggregation propensity. In our previous investigation of polyQ peptides, we examined the effect of increasing the pH to 12, where the lysines are uncharged.[40] Briefly, charge neutralization had little to no effect on shorter polyQ peptides (Q8 or Q12); there was a slight decrease in $\langle R \rangle$ for the monomer but no significant change in aggregation. As the length increased, the effect of neutralizing charge became more dramatic: the intensity of scattered light of Q20 increased 4-fold, and Q24 immediately formed insoluble precipitates. We did not attempt similar experiments with polyA; due to alanine's higher hydrophobicity compared to glutamine, we believe we would have problems with insolubility. The effect of placement of charged residues on polyalanine aggregate morphology has been examined theoretically.[84]

Comparison to PolyA Protein. It is informative to compare polyA peptides to proteins containing polyA segments. Expansion of the polyA segment in PABPN1 from A_{10} to A_{17} resulted in increased α-helicity in solution and fibrillar aggregation after incubation at physiologic temperature.[85,86] However, these studies are complicated by the fact that wild-type PABPN1 naturally oligomerizes.[87] Expansion of the wild-type A14 polyA segment in FOXL2 resulted in mislocalization and aggregation in a length-dependent manner; expansions shorter than A19 were completely benign, but longer expansions were increasingly deleterious.[88] YFP linked to A_{23} or greater formed soluble oligomers that were trypsin-resistant and toxic to cells.[7,8] Moreover, A_{23} segments were found to self-interact and oligomerize, but $A_{\leq 18}$ did not display any self-interaction.[89] Konopka et al.[17] expanded yeast Pab1 (an RNA binding protein similar to PABPN1) from 8 to 13, 15, 17, and 20 alanines. They observed length-dependent changes in formation of inclusions, insolubility, and cytotoxicity and, most curiously, proposed that the mechanism of toxicity was different for A17 than A20-expanded Pab1. This series of results is notably similar to our finding of a striking length-dependent transition in aggregation properties between $19 < N < 25$.

Our data show that at physiological conditions polyA is trapped in amorphous oligomers whereas polyQ oligomers reorganize into mature fibrils. If soluble oligomers are more toxic than fibrils, then these differences may help to explain why the threshold for disease with polyA expansion is sharper, and why expansion of polyA has more devastating consequences than even polyQ expansion. The striking differences between A19 and A25 in particular have potential biological relevance, since no polyA segment longer than $N = 20$ exists in human proteins without pathology.

AUTHOR INFORMATION

Corresponding Author

*Phone: 608-262-1587. Fax: 608-262-5434. E-mail: regina@engr.wisc.edu.

Funding

This work was supported by Grant CBET-0852278 from the National Science Foundation.

■ ACKNOWLEDGMENTS

We gratefully acknowledge advice and assistance from Gary Case, Darrell McCaslin, Randall Massey, and Bob Walters.

■ ABBREVIATIONS

CD, circular dichroism; DLS, dynamic light scattering; FRET, fluorescence resonance energy transfer; HFIP, hexafluoroisopropanol; OPMD, oculopharyngeal muscular dystrophy; PABN1, polyadenylate binding protein nuclear 1; RP-HPLC, reverse-phase high performance liquid chromatography; SEC, size exclusion chromatography; SLS, static light scattering; TEM, transmission electron microscopy; TFA, trifluoracetic acid.

■ REFERENCES

(1) Amiel, J., Trochet, D., Clement-Ziza, M., Munnich, A., and Lyonnet, S. (2004) Polyalanine expansions in human. *Hum. Mol. Genet. 13*, R235−R243.

(2) Faux, N. G., Bottomley, S. P., Lesk, A. M., Irving, J. A., Morrison, J. R., de la Banda, M. C., and Whisstock, J. C. (2005) Functional insights from the distribution and role of homopeptide repeat-containing proteins. *Genome Res. 15*, 537−551.

(3) Beysen, D., Moumne, L., Veitia, R., Peters, H., Leroy, B. P., De Paepe, A., and De Baere, E. (2008) Missense mutations in the forkhead domain of FOXL2 lead to subcellular mislocalization, protein aggregation and impaired transactivation. *Hum. Mol. Genet. 17*, 2030−2038.

(4) Brown, L. Y., and Brown, S. A. (2004) Alanine tracts: the expanding story of human illness and trinucleotide repeats. *Trends Genet. 20*, 51−58.

(5) Messaed, C., and Rouleau, G. A. (2009) Molecular mechanisms underlying polyalanine diseases. *Neurobiol. Dis. 34*, 397−405.

(6) Albrecht, A., and Mundlos, S. (2005) The other trinucleotide repeat: polyalanine expansion disorders. *Curr. Opin. Genet. Dev. 15*, 285−293.

(7) Nojima, J., Oma, Y., Futai, E., Sasagawa, N., Kuroda, R., Turk, B., and Ishiura, S. (2009) Biochemical analysis of oligomerization of expanded polyalanine repeat proteins. *J. Neurosci. Res. 87*, 2290−2296.

(8) Toriumi, K., Oma, Y., Mimoto, A., Futai, E., Sasagawa, N., Turk, B., and Ishiura, S. (2009) Polyalanine tracts directly induce the release of cytochrome c, independently of the mitochondrial permeability transition pore, leading to apoptosis. *Genes Cells 14*, 751−757.

(9) Wang, H. M., and Monteiro, M. J. (2007) Ubiquilin overexpression reduces GFP-polyalanine-induced protein aggregates and toxicity. *Exp. Cell Res. 313*, 2810−2820.

(10) Rankin, J., Wyttenbach, A., and Rubinsztein, D. C. (2000) Intracellular green fluorescent protein-polyalanine aggregates are associated with cell death. *Biochem. J. 348*, 15−19.

(11) Davies, J. E., Rose, C., Sarkar, S., and Rubinsztein, D. C. (2010) Cystamine suppresses polyalanine toxicity in a mouse model of Oculopharyngeal Muscular Dystrophy. *Sci. Transl. Med.*, .

(12) Davies, J. E., Sarkar, S., and Rubinsztein, D. C. (2006) Trehalose reduces aggregate formation and delays pathology in a transgenic mouse model of oculopharyngeal muscular dystrophy. *Hum. Mol. Genet. 15*, 23−31.

(13) Davies, J. E., Wang, L., Garcia-Oroz, L., Cook, L. J., Vacher, C., O'Donovan, D. G., and Rubinsztein, D. C. (2005) Doxycycline attenuates and delays toxicity of the oculopharyngeal muscular dystrophy mutation in transgenic mice. *Nature Med. 11*, 672−677.

(14) Messaed, C., Dion, P. A., Abu-Baker, A., Rochefort, D., Laganiere, J., Brais, B., and Rouleau, G. A. (2007) Soluble expanded PABPN1 promotes cell death in oculopharyngeal muscular dystrophy. *Neurobiol. Dis. 26*, 546−557.

(15) Fan, X. P., Dion, P., Laganiere, J., Brais, B., and Rouleau, G. A. (2001) Oligomerization of polyalanine expanded PABPN1 facilitates nuclear protein aggregation that is associated with cell death. *Hum. Mol. Genet. 10*, 2341−2351.

(16) Riley, B. E., and Orr, H. T. (2006) Polyglutamine neurodegenerative diseases and regulation of transcription: assembling the puzzle. *Genes Dev. 20*, 2183−2192.

(17) Konopka, C. A., Locke, M. N., Gallagher, P. S., Pham, N., Hart, M. P., Walker, C. J., Gitler, A. D., and Gardner, R. G. (2011) A yeast model for polyalanine-expansion aggregation and toxicity. *Mol. Biol. Cell 22*, 1971−1984.

(18) Latouche, M., Fragner, P., Martin, E., El Hachimi, K. H., Zander, C., Sittler, A., Ruberg, M., Brice, A., and Stevanin, G. (2006) Polyglutamine and polyalanine expansions in ataxin7 result in different types of aggregation and levels of toxicity. *Mol. Cell. Neurosci. 31*, 438−445.

(19) Berger, Z., Davies, J. E., Luo, S. Q., Pasco, M. Y., Majoul, I., O'Kane, C. J., and Rubinsztein, D. C. (2006) Deleterious and protective properties of an aggregate-prone protein with a polyalanine expansion. *Hum. Mol. Genet. 15*, 453−465.

(20) Levy, Y., Jortner, J., and Becker, O. M. (2001) Solvent effects on the energy landscapes and folding kinetics of polyalanine. *Proc. Natl. Acad. Sci. U. S. A. 98*, 2188−2193.

(21) Leitgeb, B., Kerenyi, A., Bogar, F., Paragi, G., Penke, B., and Rakhely, G. (2007) Studying the structural properties of polyalanine and polyglutamine peptides. *J. Mol. Model 13*, 1141−1150.

(22) Farmer, R. S., and Kiick, K. L. (2005) Conformational behavior of chemically reactive alanine-rich repetitive protein polymers. *Biomacromolecules 6*, 1531−1539.

(23) Chin, D. H., Woody, R. W., Rohl, C. A., and Baldwin, R. L. (2002) Circular dichroism spectra of short, fixed-nucleus alanine helices. *Proc. Natl. Acad. Sci. U. S. A. 99*, 15416−15421.

(24) Lapidus, L. J., Eaton, W. A., and Hofrichter, J. (2002) Measuring dynamic flexibility of the coil state of a helix-forming peptide. *J. Mol. Biol. 319*, 19−25.

(25) Scholtz, J. M., Hong, Q., York, E. J., Stewart, J. M., and Baldwin, R. L. (1991) Parameters of helix-coil transition theory for alanine-based peptide of varying chain lengths in water. *Biopolymers 31*, 1463−1470.

(26) Marqusee, S., Robbins, V. H., and Baldwin, R. L. (1989) Unusually stable helix formation in short alanine-based peptides. *Proc. Natl. Acad. Sci. U. S. A. 86*, 5286−5290.

(27) Nguyen, H. D., and Hall, C. K. (2006) Spontaneous fibril formation by polyalanines; Discontinuous molecular dynamics simulations. *J. Am. Chem. Soc. 128*, 1890−1901.

(28) Nguyen, H. D., and Hall, C. K. (2005) Kinetics of fibril formation by polyalanine peptides. *J. Biol. Chem. 280*, 9074−9082.

(29) Kameda, T., and Takada, S. (2006) Secondary structure provides a template for the folding of nearby polypeptides. *Proc. Natl. Acad. Sci. U. S. A. 103*, 17765−17770.

(30) Ma, B. Y., and Nussinov, R. (2002) Molecular dynamics simulations of alanine rich beta-sheet oligomers: Insight into amyloid formation. *Protein Sci. 11*, 2335−2350.

(31) PerezPaya, E., Forood, B., Houghten, R. A., and Blondelle, S. E. (1996) Structural characterization and 5′-mononucleotide binding of polyalanine beta-sheet complexes. *J. Mol. Recognit. 9*, 488−493.

(32) Blondelle, S. E., Forood, B., Houghten, R. A., and PerezPaya, E. (1997) Polyalanine-based peptides as models for self-associated beta-pleated-sheet complexes. *Biochemistry 36*, 8393−8400.

(33) Forood, B., Perezpaya, E., Houghten, R. A., and Blondelle, S. E. (1995) Formation of an extremely stable polyalanine beta-sheet macromolecule. *Biochem. Biophys. Res. Commun. 211*, 7−13.

(34) Shinchuk, L. M., Sharma, D., Blondelle, S. E., Reixach, N., Inouye, H., and Kirschner, D. A. (2005) Poly-(L-alanine) expansions form core beta-sheets that nucleate amyloid assembly. *Proteins: Struct., Funct., Bioinf. 61*, 579−589.

(35) Giri, K., Ghosh, U., Bhattacharyya, N. P., and Basak, S. (2003) Caspase 8 mediated apoptotic cell death induced by beta-sheet forming polyalanine peptides. *FEBS Lett. 555*, 380−384.

(36) Giri, K., Bhattacharyya, N. P., and Basak, S. (2007) pH-dependent self-assembly of polyalanine peptides. *Biophys. J. 92*, 293−302.

(37) Measey, T. J., Smith, K. B., Decatur, S. M., Zhao, L. M., Yang, G. L., and Schweitzer-Stenner, R. (2009) Self-aggregation of a polyalanine octamer promoted by its C-terminal tyrosine and probed by a strongly enhanced vibrational circular dichroism signal. *J. Am. Chem. Soc. 131*, 18218−+.
(38) Jang, S., Yuan, J. M., Shin, J., Measey, T. J., Schweitzer-Stenner, R., and Li, F. Y. (2009) Energy landscapes associated with the self-aggregation of an alanine-based oligopeptide (AAKA)(4). *J. Phys. Chem. B 113*, 6054−6061.
(39) Chen, S. M., Berthelier, V., Hamilton, J. B., O'Nuallain, B., and Wetzel, R. (2002) Amyloid-like features of polyglutamine aggregates and their assembly kinetics. *Biochemistry 41*, 7391−7399.
(40) Walters, R. H., and Murphy, R. M. (2009) Examining polyglutamine peptide length: A connection between collapsed conformations and increased aggregation. *J. Mol. Biol. 393*, 978−992.
(41) Lee, C. C., Walters, R. H., and Murphy, R. M. (2007) Reconsidering the mechanism of polyglutamine peptide aggregation. *Biochemistry 46*, 12810−12820.
(42) Warrass, R., Wieruszeski, J. M., Boutillon, C., and Lippens, G. (2000) High-resolution magic angle spinning NMR study of resin-bound polyalanine peptides. *J. Am. Chem. Soc. 122*, 1789−1795.
(43) Larsen, B. D., and Holm, A. (1994) Incomplete Fmoc deprotection in solid-phase synthesis of peptides. *Int. J. Pept. Protein Res. 43*, 1−9.
(44) Chen, S. M., and Wetzel, R. (2001) Solubilization and disaggregation of polyglutamine peptides. *Protein Sci. 10*, 887−891.
(45) Lakowicz, J. R. (2006) *Principles of Fluorescence Spectroscopy*, 3rd ed., Springer, Berlin.
(46) Wu, P. G., and Brand, L. (1994) Resonance energy-transfer − Methods and applications. *Anal. Biochem. 218*, 1−13.
(47) Murphy, R. M., and Pallitto, M. R. (2000) Probing the kinetics of beta-amyloid self-association. *J. Struct. Biol. 130*, 109−122.
(48) Burchard, W. (1983) Static and dynamic light scattering from branched polymers and bio-polymers. *Adv. Polym. Sci. 48*, 1−124.
(49) Murphy, R. M. (1997) Static and dynamic light scattering of biological macromolecules: What can we learn? *Curr. Opin. Biotechnol. 8*, 25−30.
(50) Pedersen, J. S. (1997) Analysis of small-angle scattering data from colloids and polymer solutions: modeling and least-squares fitting. *Adv. Colloid Interface Sci. 70*, 171−210.
(51) Stewart, W. E., Shon, Y., and Box, G. E. P. (1998) Discrimination and goodness of fit of multiresponse mechanistic models. *AIChE J. 44*, 1404−1412.
(52) Larsen, B. D., Christensen, D. H., Holm, A., Zillmer, R., and Nielsen, O. F. (1993) The Merrifiled peptide synthesis studied by near-infrared Fourier-transform Raman spectroscopy. *J. Am. Chem. Soc. 115*, 6247−6253.
(53) Heitmann, B., Job, G. E., Kennedy, R. J., Walker, S. M., and Kemp, D. S. (2005) Water-solubilized, cap-stabilized, helical polyalanines: Calibration standards for NMR and CD analyses. *J. Am. Chem. Soc. 127*, 1690−1704.
(54) Job, G. E., Kennedy, R. J., Heitmann, B., Miller, J. S., Walker, S. M., and Kemp, D. S. (2006) Temperature- and length-dependent energetics of formation for polyalanine helices in water: Assignment of w(Ala)(n,T) and temperature-dependent CD ellipticity standards. *J. Am. Chem. Soc. 128*, 8227−8233.
(55) Xiong, K., Asciutto, E. K., Madura, J. D., and Asher, S. A. (2009) Salt dependence of an alpha-helical peptide folding energy landscapes. *Biochemistry 48*, 10818−10826.
(56) Miller, J. S., Kennedy, R. J., and Kemp, D. S. (2001) Short, solubilized polyalanines are conformational chameleons: Exceptionally helical if N- and C-capped with helix stabilizers, weakly to moderately helical if capped with rigid spacers. *Biochemistry 40*, 305−309.
(57) Blondelle, S. E., Forood, B., Houghten, R. A., and PerezPaya, E. (1997) Secondary structure induction in aqueous vs membrane-like environments. *Biopolymers 42*, 489−498.
(58) Spek, E. J., Olson, C. A., Shi, Z. S., and Kallenbach, N. R. (1999) Alanine is an intrinsic alpha-helix stabilizing amino acid. *J. Am. Chem. Soc. 121*, 5571−5572.
(59) Shi, Z. S., Olson, C. A., Rose, G. D., Baldwin, R. L., and Kallenbach, N. R. (2002) Polyproline II structure in a sequence of seven alanine residues. *Proc. Natl. Acad. Sci. U. S. A. 99*, 9190−9195.
(60) Schweitzer-Stenner, R., and Measey, T. J. (2007) The alanine-rich XAO peptide adopts a heterogeneous population, including turn-like and polyproline II conformations. *Proc. Natl. Acad. Sci. U. S. A. 104*, 6649−6654.
(61) Verbaro, D., Ghosh, I., Nau, W. M., and Schweitzer-Stenner, R. (2010) Discrepancies between conformational distributions of a polyalanine peptide in solution obtained from Molecular Dynamics force fields and amide I ' band profiles. *J. Phys. Chem. B 114*, 17201−17208.
(62) Rossi, M., Blum, V., Kupser, P., von Helden, G., Bierau, F., Pagel, K., Meijer, G., and Scheffler, M. (2010) Secondary structure of Ac-Ala(n)-LysH(+) polyalanine peptides (n=5, 10, 15) in vacuo: helical or not? *J. Phys. Chem. Lett. 1*, 3465−3470.
(63) Oommachen, S., Ren, J. H., and McCallum, C. M. (2008) Stabilizing helical polyalanine peptides with negative polarity or charge: Capping with cysteine. *J. Phys. Chem. B 112*, 5702−5709.
(64) Han, W., and Wu, Y. D. (2007) Coarse-grained protein model coupled with a coarse-grained water model: Molecular dynamics study of polyalanine-based peptides. *J. Chem. Theory Comput. 3*, 2146−2161.
(65) Zhou, H. X. (2004) Polymer models of protein stability, folding, and interactions. *Biochemistry 43*, 2141−2154.
(66) Doi, M. (1992) *Introduction to Polymer Physics*, Oxford University Press, Oxford.
(67) Hyeon, C., Thirumalai, D. (2006) Kinetics of interior loop formation in semiflexible chains, *J. Chem. Phys.124*.
(68) Zhou, H. X. (2001) Loops in proteins can be modeled as worm-like chains. *J. Phys. Chem. B 105*, 6763−6766.
(69) Tucker, M. J., Oyola, R., and Gai, F. (2005) Conformational distribution of a 14-residue peptide in solution: A fluorescence resonance energy transfer study. *J. Phys. Chem. B 109*, 4788−4795.
(70) Buscaglia, M., Lapidus, L. J., Eaton, W. A., and Hofrichter, J. (2006) Effects of denaturants on the dynamics of loop formation in polypeptides. *Biophys. J. 91*, 276−288.
(71) Kellermayer, M. S. Z., and Bustamante, C. (1997) Folding-unfolding transitions in single titin molecules characterized with laser tweezers. *Science 277*, 1112−1117.
(72) Tzul, F. O., and Bowler, B. E. (2010) Denatured states of low-complexity polypeptide sequences differ dramatically from those of foldable sequences. *Proc. Natl. Acad. Sci. U. S. A. 107*, 11364−11369.
(73) Zhou, J., Thorpe, I. F., Izvekov, S., and Voth, G. A. (2007) Coarse-grained peptide modeling using a systematic multiscale approach. *Biophys. J. 92*, 4289−4303.
(74) Joyce, J. G., Cook, J. C., Przysiecki, C. T., and Lehman, E. D. (1994) Chromatographic separation of low-molecular-mass recombinant proteins and peptides on Superdex-30 Prep grade. *J. Chromatogr., B: Biomed. Sci. Appl. 662*, 325−334.
(75) Kuntz, I. D., and Kauzmann, W. (1974) Hydration of proteins and polypeptides. *Adv. Protein Chem. 28*, 239−345.
(76) Kuntz, I. D. (1971) Hydration of macromolecules. 3. Hydration of polypeptides. *J. Am. Chem. Soc. 93*, 514.
(77) Uversky, V. N., Gillespie, J. R., and Fink, A. L. (2000) Why are "natively unfolded" proteins unstructured under physiologic conditions? *Proteins: Struct., Funct., Genet. 41*, 415−427.
(78) Tran, H. T., Mao, A., and Pappu, R. V. (2008) Role of backbone - Solvent interactions in determining conformational equilibria of intrinsically disordered proteins. *J. Am. Chem. Soc. 130*, 7380−7392.
(79) Mao, A. H., Crick, S. L., Vitalis, A., Chicoine, C. L., and Pappu, R. V. (2010) Net charge per residue modulates conformational ensembles of intrinsically disordered proteins. *Proc. Natl. Acad. Sci. U. S. A. 107*, 8183−8188.
(80) Wright, P. E., and Dyson, H. J. (1999) Intrinsically unstructured proteins: Re-assessing the protein structure-function paradigm. *J. Mol. Biol. 293*, 321−331.
(81) Blanch, E. W., Morozova-Roche, L. A., Cochran, D. A. E., Doig, A. J., Hecht, L., and Barron, L. D. (2000) Is polyproline II helix the killer conformation? A Raman optical activity study of the

amyloidogenic prefibrillar intermediate of human lysozyme. *J. Mol. Biol. 301*, 553−563.
(82) Chi, E. Y., Krishnan, S., Randolph, T. W., and Carpenter, J. F. (2003) Physical stability of proteins in aqueous solution: Mechanism and driving forces in nonnative protein aggregation. *Pharm. Res. 20*, 1325−1336.
(83) Schmit, J. D., Ghosh, K., and Dill, K. (2011) What drives amyloid molecules to assemble into oligomers and fibrils? *Biophys. J. 100*, 450−458.
(84) Semenov, A. N., and Subbotin, A. V. (2010) Theory of self-assembling structures of model oligopeptides. *Macromolecules 43*, 3487−3501.
(85) Sackewitz, M., Von Einem, S., Hause, G., Wunderlich, M., Schmid, F. X., and Schwarz, E. (2008) A folded and functional protein domain in an amyloid-like fibril. *Protein Sci. 17*, 1044−1054.
(86) Scheuermann, T., Schulz, B., Blume, A., Wahle, E., Rudolph, R., and Schwarz, E. (2003) Trinucleotide expansions leading to an extended poly-L-alanine segment in the poly (A) binding protein PABPN1 cause fibril formation. *Protein Sci. 12*, 2685−2692.
(87) Keller, R. W., Kuhn, U., Aragon, M., Bornikova, L., Wahle, E., and Bear, D. G. (2000) The nuclear poly(A) binding protein, PABP2, forms an oligomeric particle covering the length of the poly(A) tail. *J. Mol. Biol. 297*, 569−583.
(88) Moumne, L., Dipietromaria, A., Batista, F., Kocer, A., Fellous, M., Pailhoux, E., and Veitia, R. A. (2008) Differential aggregation and functional impairment induced by polyalanine expansions in FOXL2, a transcription factor involved in cranio-facial and ovarian development. *Hum. Mol. Genet. 17*, 1010−1019.
(89) Oma, Y., Kino, Y., Toriumi, K., Sasagawa, N., and Ishiura, S. (2007) Interactions between homopolymeric amino acids (HPAAs). *Protein Sci. 16*, 2195−2204.